Stanford Exploration Project, Report 124, April 4, 2006, pages 1–??

Target-oriented wave-equation inversion with regularization in the subsurface-offset domain

Alejandro A. Valenciano

ABSTRACT

A complex velocity model can cause shadow zones in an image computed by migration due to poor illumination. These shadow zones may contain weak signals masked by artifacts. To reduce artifacts and recover the real signal, a wave-equation target-oriented inversion scheme can be developed that uses an explicitly computed least squares inversion Hessian. To solve the otherwise ill-conditioned inversion problem a model regularization needs to be added. One choice for regularization is to penalize the energy in the image not focused at zero subsurface-offset. The subsurface-offset Hessian needs to be computed by using the adjoint of migration as the modeling operator. Results on Sigsbee model show encouraging results.

INTRODUCTION

Conventional imaging techniques such as migration cannot provide an accurate picture of poorly illuminated areas (Clapp, 2005). In such areas, migration artifacts can easily obscure the small amount of signal that exists. One way to solve this problem is to use an inversion formalism introduced by Tarantola (1987) to solve geophysical imaging problems. This procedure computes an image by weighting the migration result with the inverse of the Hessian matrix.

However, when the dimensions of the problem get large, the explicit calculation of the Hessian matrix and its inverse becomes unfeasible. That is why Valenciano and Biondi (2004) and Valenciano et al. (2005b) proposed the following approximation: (1) to compute the Hessian in a target-oriented fashion to reduce the size of the problem; (2) to exploit the sparse structure of the Hessian matrix; and (3) to compute the inverse image following a iterative inversion scheme. The last item renders unnecessary an explicit computation of inverse of the Hessian matrix.

In this paper, I apply the target-oriented wave-equation inversion to the Sigsbee data set. Different to the Valenciano et al. (2005a) work, the image space now contains a subsurface-offset dimension. I compare the customary damping model regularization applied in Valenciano et al. (2005a) with a regularization that penalizes energy in the image not focused at zero subsurface-offset (Shen et al., 2003). This is possible after the theoretical definition of the subsurface-offset wave-equation Hessian (Valenciano and Biondi, 2005).

LINEAR LEAST-SQUARES INVERSION

Tarantola (1987) formalizes the geophysical inverse problem by giving a theoretical approach to compensate for experimental deficiency (e.g., acquisition geometry, complex overburden), while being consistent with the acquired data. His approach can be summarized as follows: given a linear modeling operator $\mathbf{L}$, compute synthetic data $\mathbf{d}$ using $\mathbf{d} = \mathbf{L}\mathbf{m}$ where $\mathbf{m}$ is a reflectivity model. Given the recorded data $\mathbf{d}_{obs}$, a quadratic cost function,

$$S(\mathbf{m}) = \|\mathbf{d} - \mathbf{d}_{obs}\|^2 = \|\mathbf{L}\mathbf{m} - \mathbf{d}_{obs}\|^2, \tag{1}$$

is formed. The reflectivity model $\hat{\mathbf{m}}$ that minimizes $S(\mathbf{m})$ is given by the following:

$$\hat{\mathbf{m}} = (\mathbf{L}'\mathbf{L})^{-1}\mathbf{L}'\mathbf{d}_{obs} = \mathbf{H}^{-1}\mathbf{m}_{mig}, \tag{2}$$

where $\mathbf{L}'$ (migration operator) is the adjoint of the linear modeling operator $\mathbf{L}$, $\mathbf{m}_{mig}$ is the migration image, and $\mathbf{H} = \mathbf{L}'\mathbf{L}$ is the Hessian of $S(\mathbf{m})$.

The main difficulty with this approach is the explicit calculation of the Hessian inverse. In practice, it is more feasible to compute the least-squares inverse image as the solution of the linear system of equations,

$$\mathbf{H}\hat{\mathbf{m}} = \mathbf{m}_{mig}, \tag{3}$$

by using an iterative inversion algorithm.

REGULARIZATION IN THE SUBSURFACE-OFFSET DOMAIN

Valenciano et al. (2005a) solve equation 3 in a poststack image domain (zero subsurface-offset). The authors conclude that a prestack regularization was necessary to reduce the noise in the inversion result. After Valenciano and Biondi (2005), theoretical definition of the prestack wave-equation Hessian (subsurface-offset, and reflection angle) a generalization to the prestack image domain of equation 3 is possible.

Three different regularization schemes for wave-equation inversion have been discussed in the literature. First, an identity operator which is customary in many scientific applications (damping). Second, a geophysical regularization which penalizes the roughness of the image in the offset ray parameter dimension (which is equivalent the reflection angle dimension) (Prucha et al., 2000; Kuehl and Sacchi, 2001). Third, a differential semblance operator to penalize the energy in the image not focused at zero subsurface-offset (Shen et al., 2003). In this paper I compare the first and the third regularization schemes, because a regularization in the subsurface-offset is more attractive in terms of computational cost. The regularization in the reflection angle domain will be a topic of future research.

A generalization to the prestack image domain of equation 3 needs regularization to obtain a stable solution. The first option for regularization is a customary damping that can be stated

as follows:

$$\begin{aligned} \mathbf{H}(\mathbf{x},\mathbf{h};\mathbf{x}',\mathbf{h}')\hat{\mathbf{m}}(\mathbf{x},\mathbf{h}) - \mathbf{m}_{mig}(\mathbf{x},\mathbf{h}) &\approx 0, \\ \varepsilon \mathbf{I}\hat{\mathbf{m}}(\mathbf{x},\mathbf{h}) &\approx 0, \end{aligned} \tag{4}$$

where $\mathbf{x} = (x, y, z)$ is a point in the image, and $\mathbf{h} = (h_x, h_y, h_z)$ is the half subsurface-offset. The subsurface-offset Hessian $\mathbf{H}(\mathbf{x},\mathbf{h};\mathbf{x}',\mathbf{h}')$ as define by Valenciano and Biondi (2005) is

$$\mathbf{H}(\mathbf{x},\mathbf{h};\mathbf{x}',\mathbf{h}') = \sum_{\omega} \sum_{\mathbf{x}_s} \mathbf{G}'(\mathbf{x}+\mathbf{h},\mathbf{x}_s;\omega)\mathbf{G}(\mathbf{x}'+\mathbf{h}',\mathbf{x}_s;\omega) \sum_{\mathbf{x}_r} \mathbf{G}'(\mathbf{x}-\mathbf{h},\mathbf{x}_r;\omega)\mathbf{G}(\mathbf{x}'-\mathbf{h}',\mathbf{x}_r;\omega),$$

where $\mathbf{G}(\mathbf{x},\mathbf{x}_s;\omega)$ and $\mathbf{G}(\mathbf{x},\mathbf{x}_r;\omega)$ are the Green functions from shot position $\mathbf{x}_s$ and receiver position $\mathbf{x}_r$ to a model space point $\mathbf{x}$.

The third regularization option for the prestack generalization of equation 3, is penalizing the energy in the image not focused at zero subsurface-offset. This is obtained using the fitting goals,

$$\begin{aligned} \mathbf{H}(\mathbf{x},\mathbf{h};\mathbf{x}',\mathbf{h}')\hat{\mathbf{m}}(\mathbf{x},\mathbf{h}) - \mathbf{m}_{mig}(\mathbf{x},\mathbf{h}) &\approx 0, \\ \varepsilon \mathbf{P}_{\mathbf{h}}\hat{\mathbf{m}}(\mathbf{x},\mathbf{h}) &\approx 0, \end{aligned} \tag{5}$$

where $\mathbf{P}_{\mathbf{h}} = |\mathbf{h}|$ is the differential semblance operator (Shen et al., 2003). The only difference between equations 4 and 5 is in the regularization operator.

In the next section I compare the numerical solution of the inversion problems stated in equations 4 and 5 to the imaging of Sigsbee model.

NUMERICAL RESULTS: SIGSBEE MODEL

The Sigsbee data set was modeled by simulating the geological setting found on the Sigsbee escarpment in the deep-water Gulf of Mexico. The model exhibits the illumination problems due to the complex salt shape, characterized by a rugose salt top (see Figure 1). I choose a target zone (indicated with the "target" box in Figure 1) to see the effects of illumination on imaging close to the salt body.

Figure 2 shows the shot-profile migration image (using a cross-correlation imaging condition) corresponding to the portion of Sigsbee model shown in Figure 1. Notice how the diffractor amplitudes located at 17000 feet depth fade away as they get closer to the salt boundary. The same happens to the reflectors as they get close to the salt .

Figure 3 shows the Hessian (21×7 filter coefficients) at constant depth as the x coordinate moves toward the salt boundary. The subsurface-offset is fixed at $(\mathbf{h},\mathbf{h}') = (0,0)$ feet –the center of the filter lies in the diagonal of the Hessian matrix. Figure 3a shows point 1, with coordinates $\mathbf{x_1} = (17000, 40000)$ far from the salt body. Figure 3b shows point 2, with coordinates $\mathbf{x_2} = (17000, 45000)$. Figure 3c shows point 3, with coordinates $\mathbf{x_3} = (17000, 50000)$. Figure 3d shows point 4, with coordinates $\mathbf{x_4} = (17000, 55000)$.

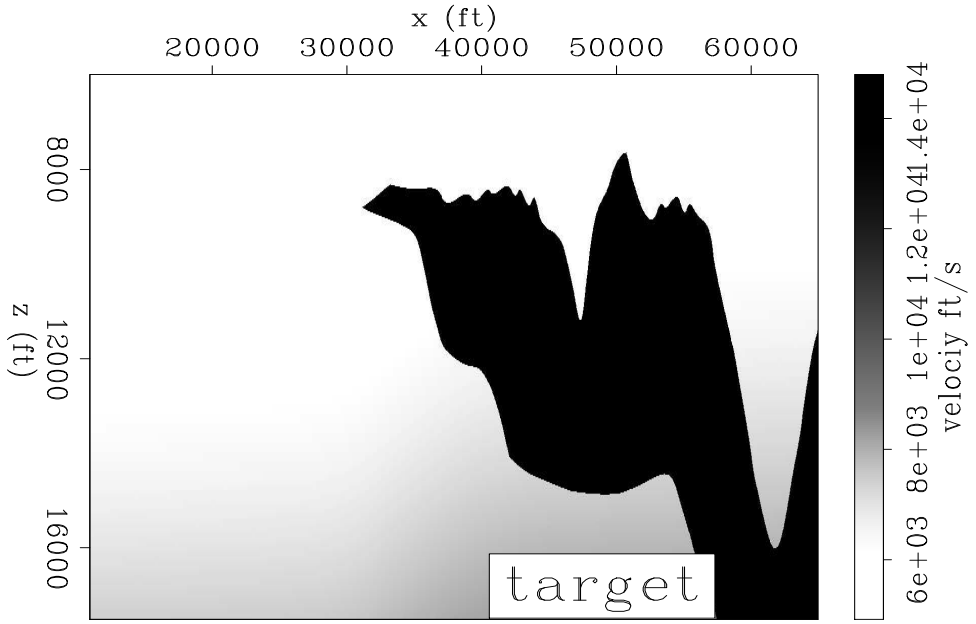

Figure 1: Sigsbee velocity model, target zone indicated with the "target" box. alejandro1-Sis_vel [CR]

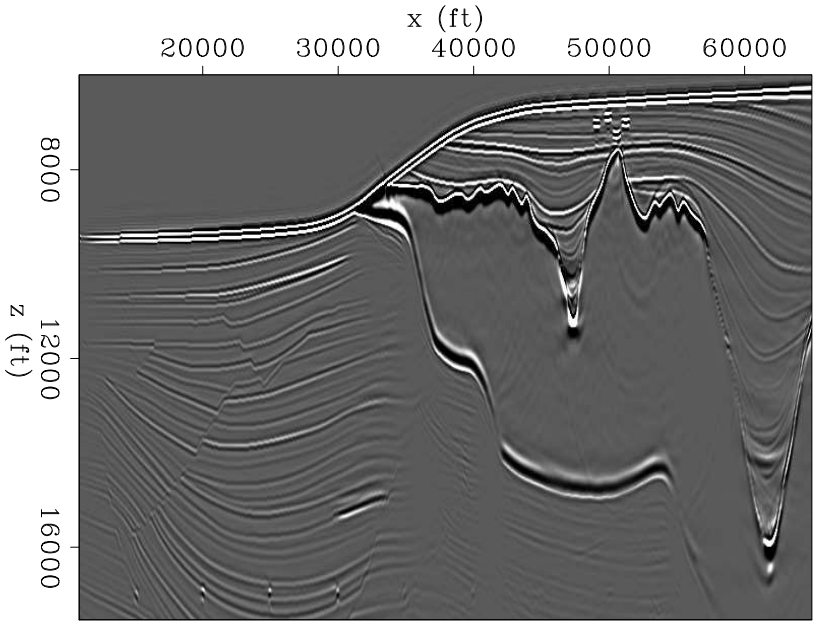

Figure 2: Sigsbee shot-profile migration image using a cross-correlation imaging condition. alejandro1-mig_Sis [CR]

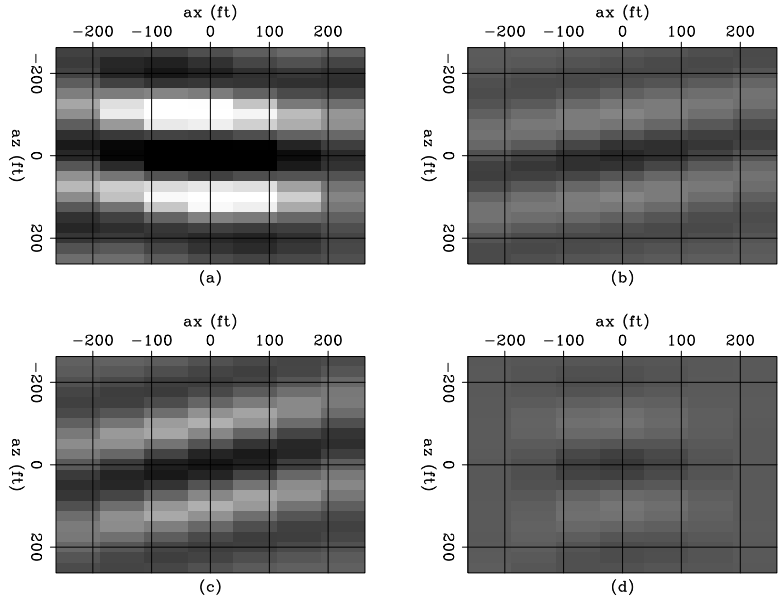

Figure 3: Hessian at zero subsurface-offset of the Sigsbee model at 4 different subsurface locations, a) $\mathbf{x_1} = (17000, 40000)$, b) $\mathbf{x_2} = (17000, 45000)$, c) $\mathbf{x_3} = (17000, 50000)$, and d) $\mathbf{x_4} = (17000, 55000)$. The filter shape changes as we get closer to the salt. alejandro1-hesian_phase_Sis [CR]

The shape of the filter depends not only on the acquisition geometry but also on the velocity model (i.e. presence of the salt body). In the area unaffected by the salt body, the filter is well behaved (Figure 3a). However, as we get closer to the salt boundary the complexity of wave propagation starts to affect the shape of the filter. In this case, the filter coefficients diminish in intensity and tilt toward the illuminated angles (Figure 3c). This is due to a focusing and defocusing effect created by the salt body.

To correct the effect of uneven illumination, the least squares image was computed. Figure 4 shows a comparison between the migration and the inversion images in the target area. The stratigraphic model is shown in Figure 4a. Notice the four equal-strength point diffractors. Figure 4b shows the illumination, which is the diagonal of the Hessian matrix (dark is high illumination, light is low illumination). Notice the decrease in the illumination as it gets closer to the salt with the exception of a narrow strip where energy focuses close to the salt. The zero subsurface-offset migration result is shown in Figure 4c. The reflectors dim out as they get closer to the salt. Notice how the diffractor amplitudes located at 17000 feet depth fade away as they get closer to the salt. The same happens to the reflectors as they get close to the salt with the exception of a narrow strip coincident with the high illumination. In contrast, Figure 4d, and 4e show the zero subsurface-offset inversion results by using equation 4, and 5 respectively. In both cases, the resolution increases (especially to the left of the image) and the section looks more balance.

Minor differences exist between Figures 4d and 4e. That is a result to be expected since the regularization described in equation 5 only penalizes the amplitudes of the image away

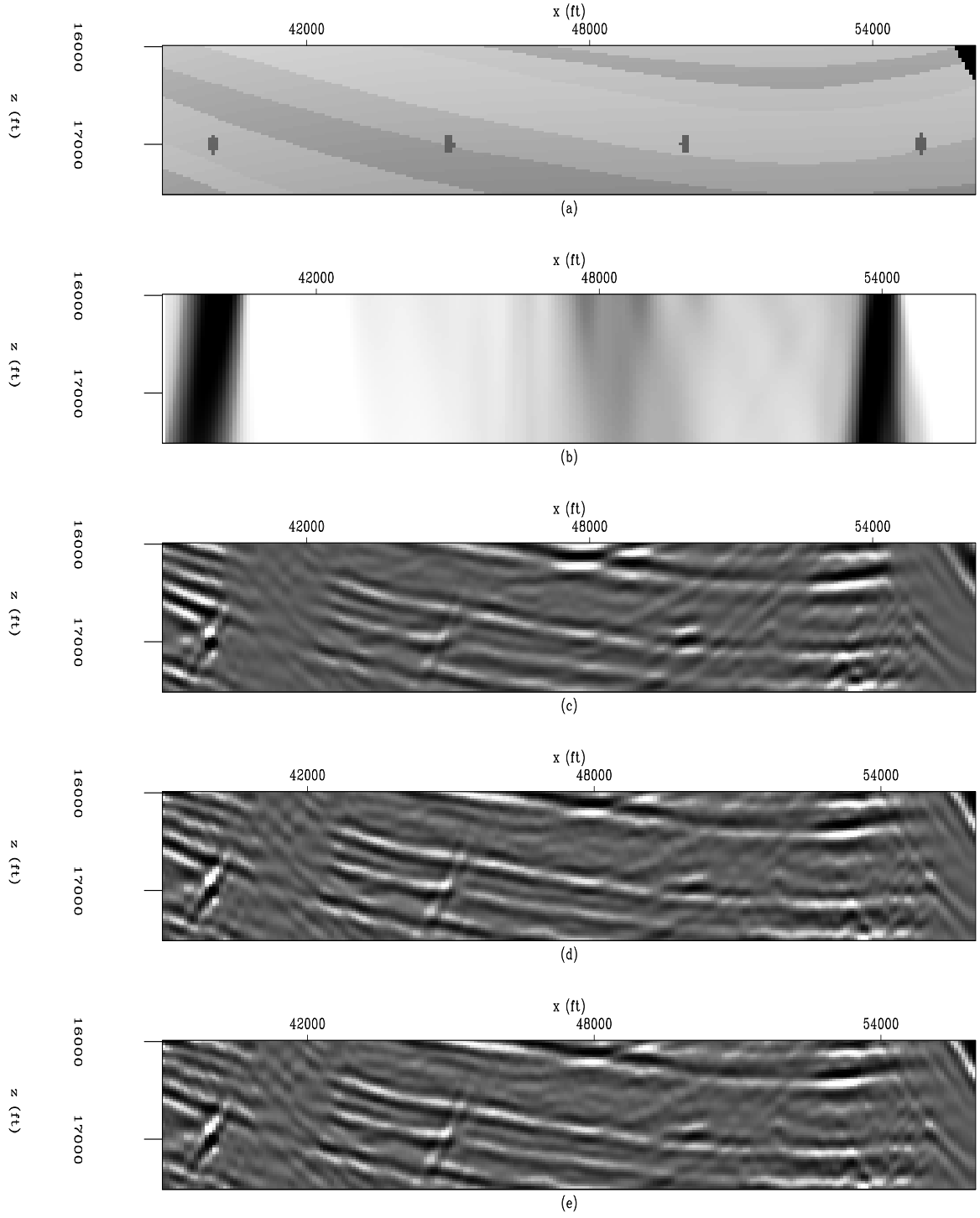

Figure 4: Target area zero subsurface-offset comparison. (a) stratigraphic model, (b) illumination (dark is high and light is low), (c) zero subsurface-offset migration, (d) zero subsurface-offset inversion with damping regularization, and (e) zero subsurface-offset inversion with regularization that penalizes the energy in the image not focused at zero subsurface-offset. alejandro1-comp_Sis_full [CR]

from zero offset. A more relevant comparison can be seen in Figures 5, 6, and 7. Where the migration image in the subsurface-offset domain is shown in Figure 5, the subsurface-offset domain inversion with a damping regularization is shown in Figure 6, and the subsurface-offset domain inversion with regularization that penalizes the energy in the image not focused at zero subsurface-offset is shown in 7. Notice how the images differ away from zero subsurface-offset, being the latest the one with the energy more focused at zero.

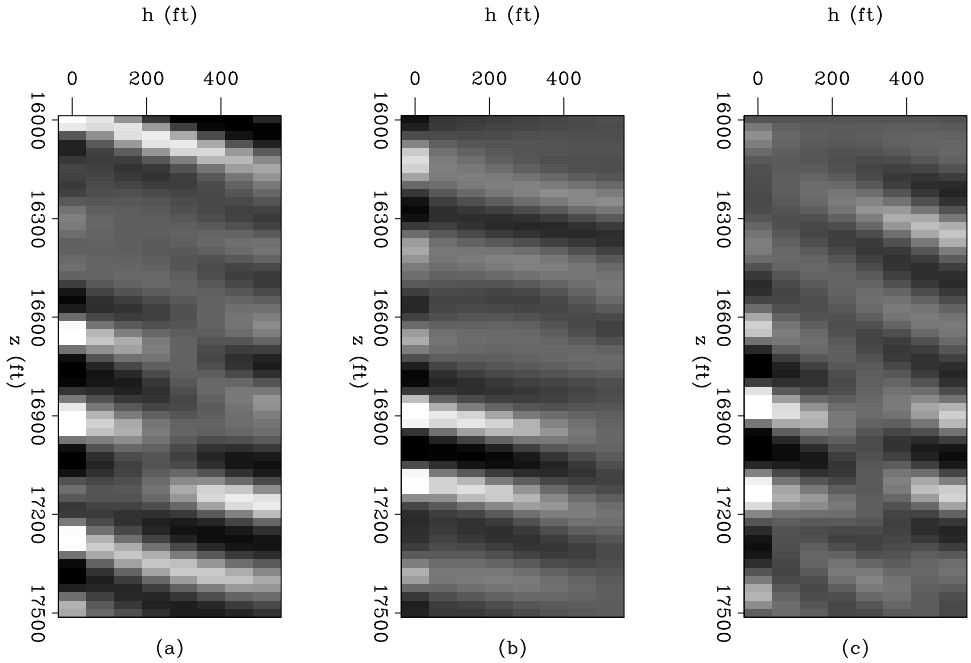

Figure 5: Commom image gathers (subsurface-offset domain) for the migration. (a) $x_1 = 45000$, (b) $x_2 = 50000$, and (c) $x_2 = 55000$. alejandro1-comp_off_mig [CR]

CONCLUSIONS AND FUTURE RESEARCH

A generalization of the wave-equation target-oriented inversion to the prestack image domain needs regularization, since the condition number of the target-oriented Hessian matrix can be high. Two prestack regularization methods to stabilize the subsurface-offset domain inversion were compared. The first, an identity operator which penalizes the size of the overall image (damping). The second, a differential semblance operator that penalizes the energy in the image not focused at zero subsurface-offset (Shen et al., 2003).

While imaging the Sigsbee model, both prestack inversion methods obtained better zero subsurface-offset images than migration, increasing the resolution and the continuity of the events into the shadow zones. The main differences between them is away from zero subsurface-offset where the the second method present less energy as imposed by the regularization.

The effects that both regularizations might produce in the angle domain image, after applying a subsurface-offset to angle transformation following (Sava and Fomel, 2003), will be a subject of future study.

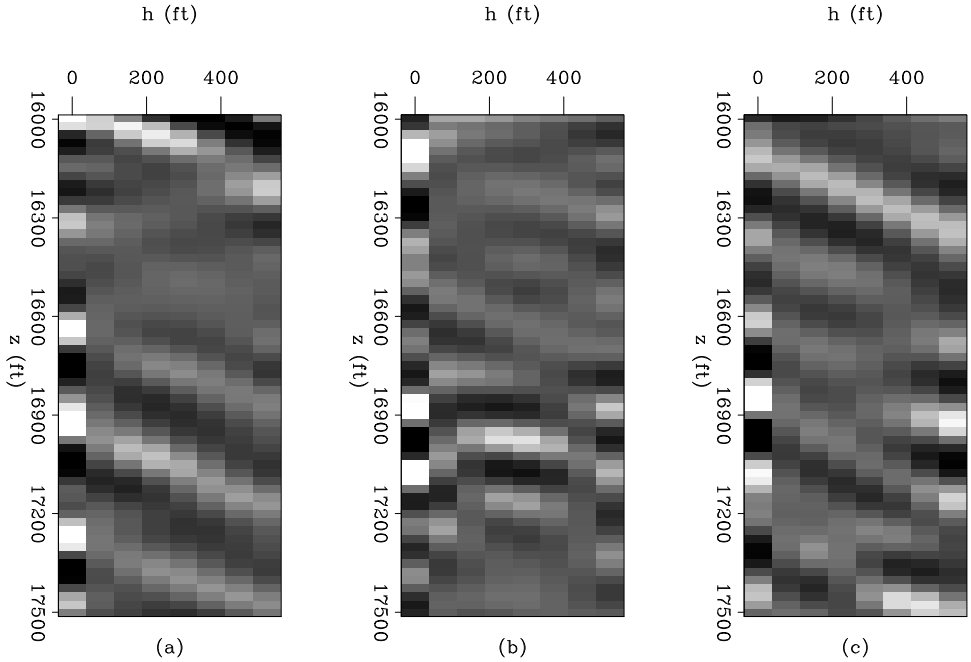

Figure 6: Commom image gathers (subsurface-offset domain) for the inversion with damping regularization. (a) $x_1 = 45000$, (b) $x_2 = 50000$, and (c) $x_2 = 55000$. alejandro1-comp_off_inv_damp [CR]

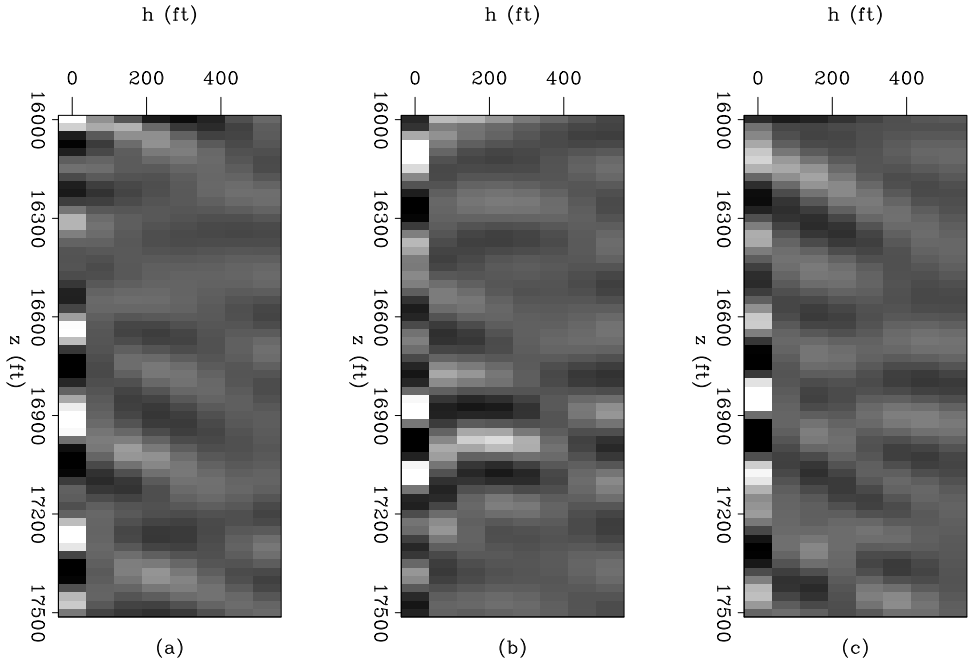

Figure 7: Commom image gathers (subsurface-offset domain) for the inversion with differential semblance regularization. (a) $x_1 = 45000$, (b) $x_2 = 50000$, and (c) $x_2 = 55000$. alejandro1-comp_off_inv_semb [CR]

ACKNOWLEDGMENTS

I would like to thank Gabriel Alvarez for many insightful discussions, and Robert Clapp for helping with the computational efficiency of the Hessian program.

REFERENCES

Clapp, M. L., 2005, Imaging under salt: illumination compensation by regularized inversion: Ph.D. thesis, Stanford University.

Kuehl, H. and M. Sacchi, 2001, Generalized least-squares DSR migration using a common angle imaging condtion: Soc. of Expl. Geophys., 71st Ann. Internat. Mtg, 1025–1028.

Prucha, M. L., R. G. Clapp, and B. Biondi, 2000, Seismic image regularization in the reflection angle domain: SEP–**103**, 109–119.

Sava, P. and S. Fomel, 2003, Angle-domain common-image gathers by wavefield continuation methods: Geophysics, **68**, 1065–1074.

Shen, P., W. Symes, and C. C. Stolk, 2003, Differential semblance velocity analysis by wave-equation migration: 73st Annual International Meeting, SEG, Expanded Abstracts, 2132–2135.

Tarantola, A., 1987, Inverse problem theory: Methods for data fitting and model parameter estimation: Elsevier Science Publication Company, Inc.

Valenciano, A. A. and B. Biondi, 2004, Target-oriented computation of the wave-equation imaging Hessian: SEP–**117**, 63–76.

Valenciano, A. A. and B. Biondi, 2005, Wave-equation angle-domain hessian: SEP–**123**.

Valenciano, A. A., B. Biondi, and A. Guitton, 2005a, Target-oriented wave-equation inversion: Sigsbee model: SEP–**123**.

Valenciano, A. A., B. Biondi, and A. Guitton, 2005b, Target-oriented wave-equation inversion: SEP–**120**, 23–40.